Modification of Al Surface via Acidic Treatment and its Impact on Plating and Stripping

Fatemehsadat Rahide,*[a] Krishnaveni Palanisamy,[b] Jackson K. Flowers,[c, d] Junjie Hao,[a] Helge S. Stein,[c, d, e] Christine Kranz,[b] Helmut Ehrenberg,[a, d] and Sonia Dsoke*[a, f, g]

Amorphous Al_2O_3 film that naturally exists on any Al substrate is a critical bottleneck for the cyclic performance of metallic Al in rechargeable Al batteries. The so-called electron/ion insulator Al oxide slows down the anode's activation and hinders Al plating/stripping. The Al_2O_3 film induces different surface properties (roughness and microstructure) on the metal. Al foils present two optically different sides (shiny and non-shiny), but their surface properties and influence on plating and stripping have not been studied so far. Compared to the shiny side, the non-shiny one has a higher (~28%) surface roughness, and its greater concentration of active sites (for Al plating and stripping) yields higher current densities. Immersion pretreat-ments in Ionic-Liquid/$AlCl_3$-based electrolyte with various durations modify the surface properties of each side, forming an electrode-electrolyte interphase layer rich in Al, Cl, and N. The created interphase layer provides more tunneling paths for better Al diffusion upon plating and stripping. After 500 cycles, dendritic Al deposition, generated active sites, and the continu-ous removal of the Al metal and oxide cause accelerated local corrosion and electrode pulverization. We highlight the me-chanical surface properties of cycled Al foil, considering the role of immersion pretreatment and the differences between the two sides.

Introduction

Lithium-ion batteries (LIBs) dominate the battery industry;[1] however, the limited Li supplies and safety issues related to their volatile organic electrolytes enforce the search for alternatives.[2,3] Rechargeable aluminum batteries (RABs) as a potential substitute for LIBs are associated with two electro-chemical mechanisms; 1) conversion or intercalation at the cathode and 2) reversible Al dissolution and deposition at the Al metal anode during charge and discharge.[4,5] Al metals are employed as anodes for RABs in the form of plates, foils, or particles.[5] The main outstanding features of RABs are attribut-able to the optimal Al metal anode's special qualities, like its abundance, low cost,[4,5] gravimetric capacity (2980 mAh g^{-1}),[6] and high volumetric capacity 8040 mAh cm^{-3} (four times higher than metallic Li). Al has a standard reduction potential of -1.66 V (vs. SHE), and can transfer 3 electrons.[5,7]

However, applying metallic Al as an anode in RABs presents issues such as volume expansion, insulating passive film formation, and self-corrosion.[5] Al purity, Al dendrites formation, Al_2O_3 oxide films, grain size, crystal orientation, and microstructure[5] affect the Al anode's performance. Low Al anode efficiency is caused by impurities such as iron, silicon, and copper that can create localized galvanic cells as cathodic

[a] F. Rahide, J. Hao, Prof. Dr. H. Ehrenberg, Prof. Dr. S. Dsoke
Institute for Applied Materials (IAM)
Karlsruhe Institute of Technology (KIT)
Hermann-von-Helmholtz-Platz 1, 76344 Eggenstein-Leopoldshafen (Ger-many)
E-mail: fatemehsadat.rahide@kit.edu
sonia.dsoke@kit.edu

[b] K. Palanisamy, Prof. Dr. C. Kranz
Institute of Analytical and Bioanalytical Chemistry
Ulm University
Albert-Einstein-Allee 11, 89081 Ulm (Germany)

[c] J. K. Flowers, Prof. Dr. H. S. Stein
Institute of Physical Chemistry (IPC)
Karlsruhe Institute of Technology (KIT)
Fritz-Haber Weg 2, 76131 Karlsruhe (Germany)

[d] J. K. Flowers, Prof. Dr. H. S. Stein, Prof. Dr. H. Ehrenberg
Helmholtz Institute Ulm (HIU)
Helmholtzstr. 11, 89081 Ulm (Germany)

[e] Prof. Dr. H. S. Stein
Current Address
Department of Chemistry
Technical University of Munich
Lichtenbergstr. 4, 85748 Garching b. München (Germany)

[f] Prof. Dr. S. Dsoke
Current Address
Fraunhofer Institute for Solar Energy Systems
Heidenhofstr. 2, 79110 Freiburg (Germany)

[g] Prof. Dr. S. Dsoke
Current Address
Department of Sustainable Systems Engineering (INATECH)
University of Freiburg
79110 Freiburg (Germany)

ChemSusChem

Research Article
doi.org/10.1002/cssc.202301142

Chemistry
Europe
European Chemical
Societies Publishing

sites with Al and speed up the self-corrosion rate.[8,9] However, high purity results in a higher cost of the Al anode,[9] enforcing a performance and cost trade-off. In addition, dendritic deposition of Al occurs during repeated Al plating/stripping.[10,11] Al dendrites may puncture the separator, resulting in anode disintegration and consequent cell failure.[12] Another issue is that the Al active material is lost when dead Al dendrites peel off from the Al matrix.[13] Although the existence of Al dendrite is still under debate,[14,15] they are indeed present but restricted under the barrier of Al_2O_3, contrary to the expected dendrite-free behavior.[13] The native Al_2O_3 film hinders Al dendrite growth and subsequently stabilizes the anode/electrolyte interface.[13,16] However, the Al_2O_3 film delays the anode's activation and makes it harder to reach the reversible potential, leading to a significant overpotential or passivation.[5,6] The amorphous Al_2O_3 is an electron/ion insulator, characterized by defects and a thickness of about several nanometers allowing electron tunneling for ion conduction and charge transfer.[6,12] However, the relation between the oxide film and the Al deposition is still a matter of debate.[13,17,18]

It is reported that to activate the Al electrode/electrolyte interface, pretreatment of the Al metal anode facilitates the partial removal of the Al_2O_3 film.[12] Nevertheless, any increase in potential achieved after oxide removal could be accompanied by corrosion.[6] She et al.[19] reported that the surface evolution of the Al electrode is caused by electrochemical corrosion, which affects the Al electrode's morphological characteristics. In terms of altering the ion concentration and current distribution, the activity of the Al dendrite and size distribution also affect the Al electrode surface evolution.[19] Therefore, the pretreatment of the Al anode should be engineered to increase the active surface area of the Al anode and the capacity of Al deposition and dissolution, on top of controlling corrosion and dendrite growth.[12] Pretreatments of the Al anode can be classified as either acid etching pretreatment or electropolishing. The removal of the Al_2O_3 film increases the electrochemically active surface area of Al metal, but it also results in a weaker or less stable solid electrolyte interphase (SEI).[20,21] The pretreated Al has numerous pits that serve as active sites during the charge/discharge.[22] Acidic etching, i.e. (pre)immersion in a chloroaluminate-based ionic liquid electrolyte (ILE)[23] partially removes and modifies the surface oxide film for targeted electrochemical reactions.[24,25] However, strong protic acid etching[13] as well as electro-polishing[26] lead to the complete removal of native surface oxide film with consequent dendritic Al electrodeposition, metal anode cracking, severe corrosion, and even Al anode pulverization.[24,27] Zhan et al. examined aluminum surface activation in an acidic environment by immersing Al wools in $NaAlCl_4$ at 190 °C for 48 h, revealing Al_2O_3 passivation layer degradation.[28] Wu *et al.*[29] revealed that moderate removal of the Al_2O_3 film increases the coulombic efficiency (CE) of Al plating and stripping, whereas extreme removal indicated no improvement. The immersion duration impacts the degree of Al_2O_3 removal and the activation of the Al surface for electrochemical reactions and stabilization of the anode/electrolyte interface.[30] According to Yang *et al.*, 6 h (h) immersion time is the optimal duration in 1-butyl-3-meth-

ylimidazolium chloride ([BMIM]Cl):$AlCl_3$ (1:1.1) electrolyte.[24] ILE are known for their unique properties, including wide potential window, high ionic conductivity and low vapor pressures,[31,32] and nonvolatile and nonflammable.[33] 1-Ethyl-3-methylimidazolium chloride ([EMIm]Cl):$AlCl_3$ ILE is the most widely utilized electrolyte for enabling reversible Al plating and stripping[18,34] with good ionic conductivity.[35] [EMIm]Cl:$AlCl_3$ (1:1.5), as a conventional ILE mixture for RABs is a Lewis acid (achievable only when the molar ratio $AlCl_3$: [EMIm]Cl is >1). The chloroaluminate complexes present with this molar ratio ($Al_2Cl_7^-$) attack the surface of metallic Al, consequently causing a galvanic corrosion reaction and creating an interphase layer containing a modified passivation film (Al_2O_3).[36] Al surface is hence locally dissolved during Al plating/stripping in the ILE.[37] Furthermore, new passivation layers develop under open circuit voltage conditions as a result of the deposition of ILE decomposition products.[38] The newly formed passivation layer provides some protection, but it eventually corrodes and dissolves,[16,17,39] causing a heterogeneous distribution of species and re-structuring of the electrode, such as a change in porosity, which affects both the interfacial resistance and diffusion of the ionic species. Lee et al.[39] analyzed the morphological changes on the Al surface to explore the chemical activity and stability of Al in ILs. However, they illustrated the morphological change on the Al metal surface only qualitatively, without a detailed surface analysis.[39] It is observed that the initial passivation layer formed when in contact with ILE exhibits a porous and complex structure. This layer consists of an outer inorganic/organic component and an inner layer rich in oxides. Additionally, under open circuit voltage conditions, this layer undergoes growth through the simultaneous dissolution and redeposition of dissolved substances. During galvanostatic cycling, this phenomenon is exacerbated by electrochemical etching, which leads to the formation of pits and corrosion of the Al surface.[38] In sum, the surface properties, structure, and topology of the interfacial layers are still poorly understood. The native Al_2O_3 film has a complicated composition and nature, which is directly influenced by the manufacturing and storage conditions.[40] The temperature and humidity of storage and manufacturing places govern how adsorbed species like water, hydroxides, and carbon dioxide affect the Al_2O_3 film composition. Al_2O_3 film in contact with an ILE creates a porous film with a complex character, consisting of an inner layer rich in oxides and an outer layer of inorganic/organic materials.[38] This porous film expands when exposed to open circuit voltage by simultaneously re-depositing and dissolving deposited products, while galvanostatic cycling causes pitting corrosion of the Al metal due to electrochemical etching.[38]

A thorough understanding of the microstructure modifications and surface properties of pretreated Al foil as well as its electrochemical performance, are missing. There is a lack of a systematic study of the relation between the Al surface properties and Al microstructure changes with the reversibility and stability of the Al plating/stripping.

In this study, we highlight the correlation of different electrochemical behaviors of each side of the Al foil with their

ChemSusChem

Research Article
doi.org/10.1002/cssc.202301142

**Chemistry
Europe**
European Chemical
Societies Publishing

distinct surface properties. Moreover, we analyzed the effect of immersion pretreatment on the mechanical surface properties of the Al foil after cyclic voltammetry compared to the pristine sample. The Al surface modification, particularly the Al surface composition and microstructure modification, affects the Al electrode electrochemical performance and aging. The optimization of the Al surface (in terms of microstructure modification) has a direct impact on the kinetics of Al deposition/dissolution and cycle stability. To the best of our knowledge, the literature lacks detailed electrochemical studies of different sides of the Al foil. Typically, one side is only investigated rather than analyzing its performance differences with the other side.[41] This study presents novel insights into the surface properties changes and highlights how different sides of the Al foil undergo microstructure changes after pretreatment and cycling in [EMIm]Cl/AlCl$_3$ (1:1.5) ILE.

Results and Discussion

Each commercial Al foil has two sides with different mechanical surface properties like roughness and microstructures as a result of the manufacturing process condition.[40,42] These two different surfaces can be optically seen as shiny (Al-SH) and non-shiny (Al-NSH) with their distinct Al$_2$O$_3$ film nature and composition. The pristine Al foil was measured as received without any pretreatment. Each side of the pristine Al foil has a distinct surface morphology, as confirmed by SEM images in Figure 1. The quantity of Al, C, and O elements is presented by the EDX results. The different thicknesses and compositions of Al$_2$O$_3$ film can be related to the varied amounts of Al and O. Figure 2 shows the AFM images of pristine Al-NSH and Al-SH sides. Different surface microstructure and roughness are observed for each side. The Al-NSH side has a higher S_a compared to Al-SH. The AFM images were taken at three different spots (30 X 30 μm^2) of the Al foils. The average S_a values are given in the bar graph shown in Figure 2b. S_a, values of 123 ± 11 nm ($n = 3$) and 89 ± 7 nm ($n = 3$) were determined for Al-NSH and Al-SH, respectively. The S_a of Al-NSH have higher S_a than Al-SH side.

Regarding the electrochemical study of Al plating and stripping on Al foil, [EMIm]Cl/AlCl$_3$ (1:1.5) ILE was utilized. The electrochemical behavior of the ionic liquid mixture crucially depends on its Lewis acidity, governing efficient aluminum deposition and stripping. Achieving this involves reducing the Al$_2$Cl$_7^-$ anion at approximately -0.2 V vs. Al in strongly Lewis acidic conditions.[43–45] In ionic liquids with excess AlCl$_3$ relative to [EMIM]Cl, both AlCl$_4^-$ and Al$_2$Cl$_7^-$ ions coexist. However, only Al$_2$Cl$_7^-$ ions enable aluminum electroplating.[46–49] This electroplating occurs exclusively in acidic chloroaluminate melts with excess AlCl$_3$ and the specific capacity in the acidic melt depends on the Al$_2$Cl$_7^-$ ion concentration.[44] Reduction in the Al$_2$Cl$_7^-$ ion concentration halts both electroplating and charging processes at the cathode, resulting in a neutral melt with a 1:1 AlCl$_3$ to [EMIM]Cl ratio.[44]

Figure 3 shows CVs recorded on the two sides at the scan rate of 20 mV s^{-1} in the [EMIm]Cl/AlCl$_3$ (1:1.5) ILE. As shown in Figure 3a, an increase in current density with cycle number is observed. Independent of the side, Al$_2$O$_3$ film prevents the optimum Al deposition or dissolution, causing very low current density at the first cycle. The reason is that the oxide film hinders the electrochemically active surface area and makes it more difficult for the aluminum chloride complexes to reach the Al surface. It takes a few initial cycles to initiate electrochemical activity, during which the native Al$_2$O$_3$ film is gradually removed and dissolved in the ILE, leading to an increase in current density with cycle number. Therefore, lower current
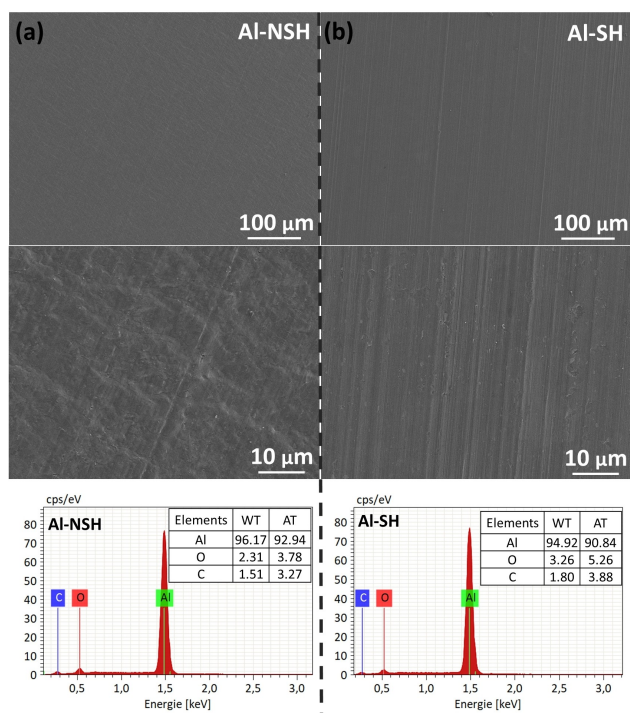

Figure 1. SEM images and EDX results and observed elements on the surface of the pristine (a) Al-NSH, and (b) Al-SH.
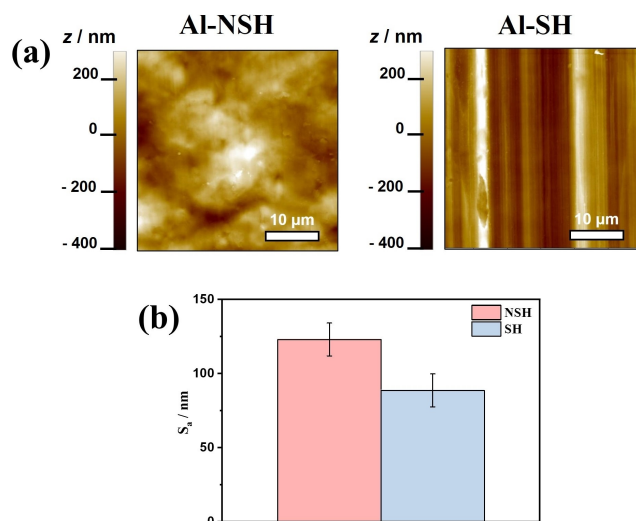

Figure 2. (a) AFM surface topography of the pristine Al-NSH and Al-SH recorded in Ar atmosphere. (b) Bar graph of mean S_a values for Al-NSH and Al-SH. Error bars reflect standard deviations from data for three different spots at one sample.
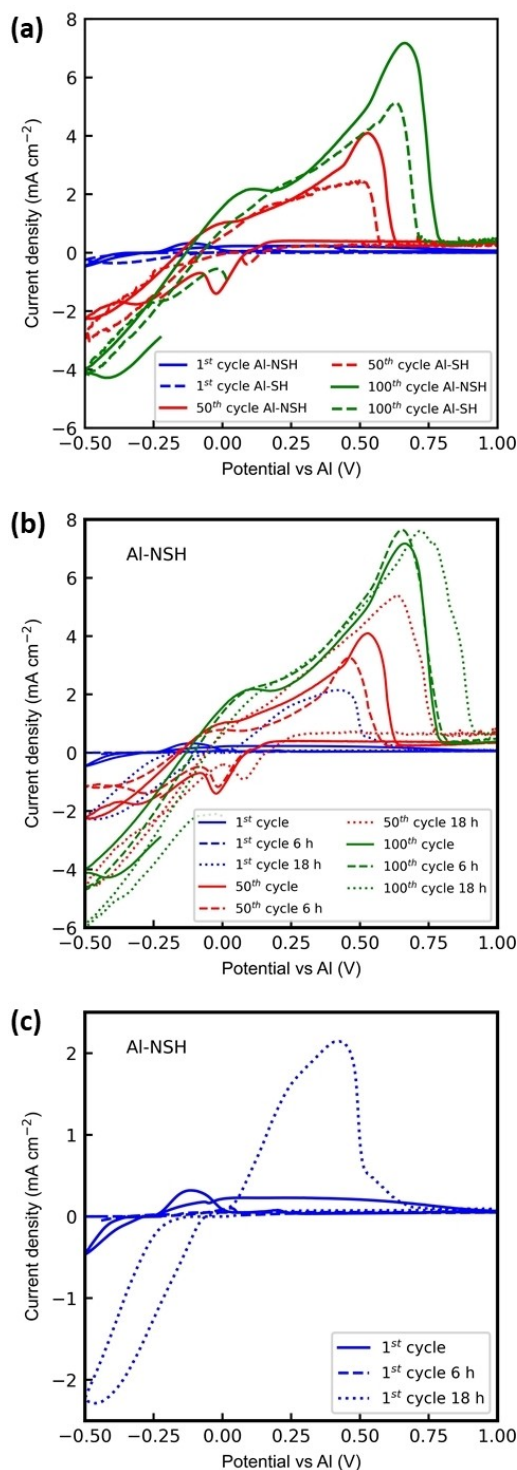
ChemSusChem

Research Article
doi.org/10.1002/cssc.202301142

Chemistry
Europe
European Chemical
Societies Publishing

Figure 3. CVs recorded on (a) pristine Al-SH and Al-NSH and (b - c) Al-NSH-6 h and Al-NSH-18 h in [EMIm]Cl/AlCl$_3$ ILE.

densities are observed for the first cycle compared to the last one (Figure 3). This phenomenon agrees with the literature, where the Al plating/stripping peaks are also reported to be small, and random during the initial cycles, but they increase and become reversible with cycling.[50,51] The recorded CV of either side shows that the current density increases with cycling

(Figure 3a), achieving a higher Al plating/stripping capacity. The current density of Al plating/stripping has a direct relation with capacity that indicates the current flow through the active surface area. The current flow depends on the initial surface properties of Al foil. Hence, the observed different current densities for each side depend on the different thicknesses and the nature of the passivation layer (Figure 3a and b). The local dissolution of the Al$_2$O$_3$ film i.e., changes in surface properties, creates active sites that govern the degree of the reversibility of Al plating/stripping as well as electrode aging. The Al-SH with a lower surface roughness indicates either homogenous Al$_2$O$_3$ film or fewer defects, which results in a blocked tunneling path for Al deposition or dissolution at the electrode/electrolyte interface, explaining the reason behind the lower current densities of Al-SH (Figure 3a). In agreement with CVs results, SEM images (Figure 4a and b) of the cycled Al-NSH exhibit more morphological surface changes, as this side is attacked strongly by the chloroaluminate Al$_2$Cl$_7^-$ anion during Al electrodeposition owing to more surface roughness. The observed rock-shape morphology for the cycled Al-NSH (Figure 4a) is correlated to the higher surface roughness of its initial surface and the wider current flow distribution caused by the presence of more active sites.

Concerning the Al surface modification, the effectiveness of the Al$_2$O$_3$ film removal depends on the mass and molar ratio of
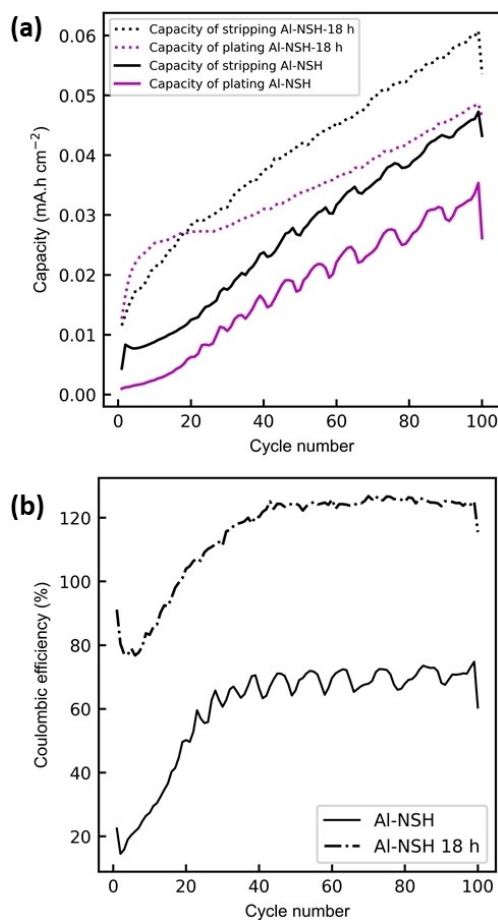

Figure 4. SEM images of the cycled (a) Al-NSH and (b) Al-SH.

ChemSusChem

Research Article
doi.org/10.1002/cssc.202301142

Chemistry
Europe
European Chemical
Societies Publishing

[EMIm]Cl/AlCl$_3$ ILE, immersion duration, and initial surface properties of the Al electrode. In order to avoid galvanic corrosion and continuous surface attack by the chloroaluminate complexes, the pretreated Al foils were washed and vacuum-dried before the electrochemical study. When the Al foil is immersed in ILE, spontaneous redox reactions occur at the electrode/electrolyte interface, creating an interphase layer. Both sides of the pretreated Al foil reveal surface morphology and roughness changes, as seen in SEM pictures (Figure S1 in the Supporting Information). Contrary to the pristine Al foil, the pretreated foil shows a relatively rough and rocky surface regardless of the side. The EDX results and observed elements on either side of the pretreated Al foil are given in Figure S2. The surfaces of the pretreated Al foil showed distinct micro-structures on both sides (Figure S3a and b), which are expected to have different surface topography, roughness, morphology, and microstructure with respect to the pristine Al foil. In the case of Al-NSH, the S_a slightly decreases in the pristine sample (123 ± 11 nm ($n = 3$)) to 102 ± 15 nm and 105 ± 7 nm, for 6 and 18 h immersion pretreatment, respectively. The reason could be associated with the partial removal of the Al$_2$O$_3$ layer from the surface of the Al-NSH surface, which apparently results in this slight decrease in S_a values. Interestingly, for Al-SH, the S_a increases to 142 ± 14 nm ($n = 3$) after 6 h immersion pretreatment and to 189 ± 11 nm ($n = 3$) after 18 h immersion pretreatment (Figure S3c). It appears that the Al$_2$O$_3$ film on the surface of the Al foil has been removed by ILE, and may have already resulted in corrosion, indicated by the notable increase in S_a. Further electrochemical studies have been carried out on Al-NSH as the observed high current density indicates more active sites originating from its initial surface properties. Moreover, less severe pitting corrosion occurs on the surface as it is assumed that the current is distributed more broadly and homogeneously. Figure 3b shows the recorded CVs on the pretreated Al-NSH compared to pristine. Independent of being pretreated or not, the current density of Al plating/stripping increases by cycle number. However, in the first cycle, the higher current density of Al-NSH-18 h compared to Al-NSH-6 h proved the facilitated Al plating/stripping.

Figure 3c reveals the importance of the immersion pretreatment on the accelerated kinetic of the Al redox reaction as the modified Al surface is rich in Al, N, O, Cl (Figure 6) with more active sites. The created active sites formed an interphase layer rich in elements like Al, N, O, and Cl are crucial for Al ion redox reactions. As immersion duration increases, surface modification intensifies, yielding more active sites. Consequently, during CV, Al foils subjected to longer immersion exhibit heightened reactivity, reflected in more pronounced peaks and increased current densities in the CV profiles. Compared to the pristine Al-NSH, the higher current density at the first cycle of Al-NSH-18 h implies the paved path for ions movement and higher Al plating/stripping capacity (Figure 5a). Fluctuations in Al plating and stripping cycle capacity stem from several factors. Repeated cycles create an electrode-electrolyte interphase layer on the electrode's surface, composed of various reaction products. This evolving layer affects ion and electron transport, causing capacity fluctuations. Side reactions, such as AlCl$_3$ formation
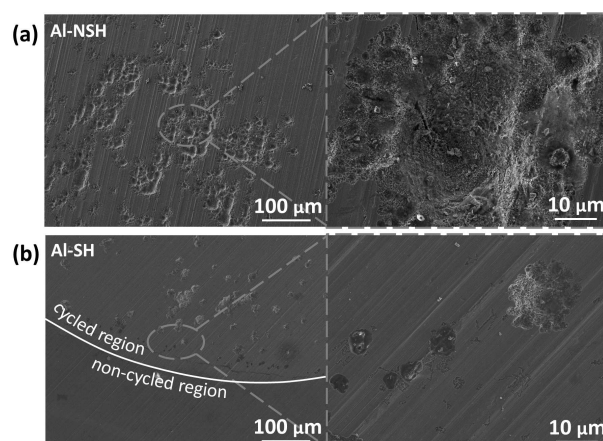

Figure 5. (a) Al plating/stripping capacity of the pristine Al-NSH and Al-NSH-18 h. (b) corresponding CE.
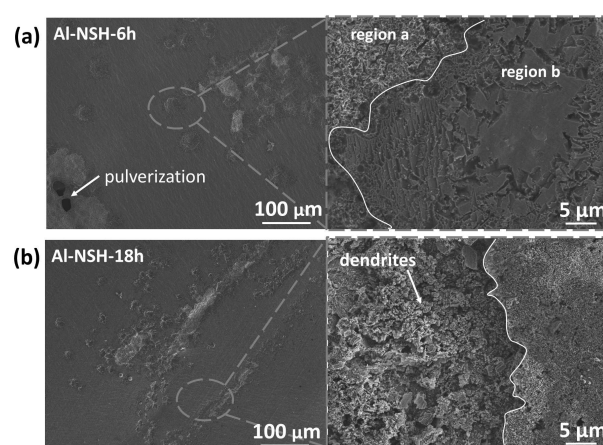

Figure 6. SEM images of cycled (a) Al-NSH-6 h, and (b) Al-NSH-18 h.

(Figure 7), and dendrite growth during plating (Figure 6), amplify these fluctuations. Additionally, mechanical stress over repeated cycles can lead to structural changes in the electrode, further contributing to capacity variations. The corresponding coulombic efficiencies are presented in Figure 5b. The coulombic efficiency of Al-NSH-18 h exhibits greater stability with fewer fluctuations compared to pristine Al-NSH, as demonstrated by Figure 5b. Moreover, Al-NSH-18 h displays a higher coulombic efficiency (at the first 10 cycles, it reaches about 80 %).

The observed pitting corrosion (Figure 6) on cycled pretreated Al foil correlates with the time that the surfaces are in contact with the electrolyte as well as generated electrochemical reactions by applied potential. Consistently with CVs, SEM images (Figure 6a and b) reveal that the longer immersion results in more Al and Al$_2$O$_3$ film dissolution and also more flaws, cracks, and defects on the surface. The immersion pretreatment creates more active sites for Al electrodeposition and dissolution and less deep pitting corrosion. In addition, the created defects on the surface facilitate Al electrodeposition and dissolution. Contrary to longer immersion, the 6 h immersion results in more localized deep pitting corrosion (e.g., see compared regions a and b in Figure 6a). Moreover, addi-
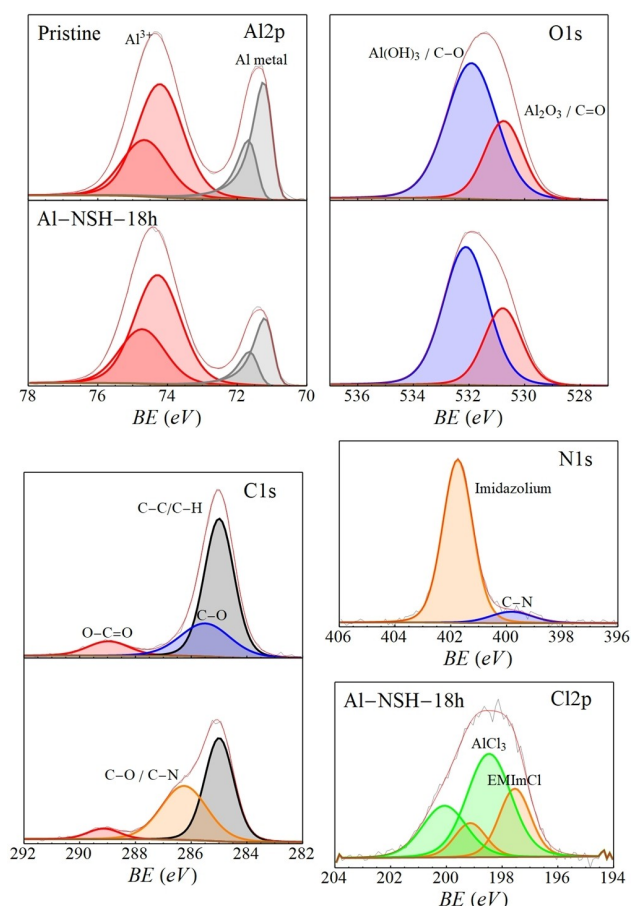
ChemSusChem

Research Article
doi.org/10.1002/cssc.202301142

Chemistry
Europe
European Chemical
Societies Publishing

Figure 7. XPS fine spectra with peak assignments for pristine Al-NSH and Al-NSH-18 h. Cl2p and N1s were taken only for Al-NSH-18 h. Spectra from the same element are normalized on the same intensity scale.

tional Al metal is pulverized as a result of localized Al metal use during cycling.

Ex-situ XPS was performed on pristine Al foil and on Al-NSH-18 h. For each sample, several survey spectra were collected to confirm the homogeneity of the surface, and then one set of fine spectra was taken. For the pristine Al-NSH, fine spectra of O1s, C1s, and Al2p were collected. For Al-NSH-18 h, fine spectra of N1s and Cl2p were also collected, and of an F1s peak, apparently due to contamination. CasaXPS was used to fit spectra[52] and calibration was performed by setting the C–C peak to 285 eV. Peaks were fit using a Shirley background, and the CasaXPS LA lineshape was used for all peaks, with an ad-hoc asymmetric shape constructed for the conductive Al metal peaks. Each O1s spectrum is fit with two peaks, each C1s spectrum with three, and each Al2p spectrum with two doublets. For the O1s spectra, the two peaks are found at roughly 531 eV and 532 eV, and correspond primarily to Al(OH)$_3$ and Al$_2$O$_3$ respectively.[49] The areal ratio between these is roughly 30:70 on both the pristine and pretreated electrodes, and the total intensity is also similar. This implies that the regrown oxide layer is of similar composition and thickness to that of the pristine foil, and that the character of the surface Al is primarily oxide, not chloride. However, the intricate composi-

tion of the oxide passivation layer on the Al metal surface is susceptible to alterations caused by storage conditions.[40,53] Factors such as temperature and humidity impact the absorption of elements like water, hydroxides, and carbon dioxide, thereby influencing the layer's overall composition.[40] The C1s spectrum of the pristine sample shows the expected hydrocarbon contamination layer, with C–C, C–O, and O–C=O peaks, at roughly 285 eV, 286 eV, and 289 eV, respectively. The peak at 286 eV substantially increases in size and shifts to slightly higher binding energy in Al-NSH-18 h, where it also accounts for C–N bonds in the imidazolium electrolyte on the surface.[54] The Al2p spectra each have a pair of doublets, with Al2p$_{3/2}$ peaks at around 71 eV and 74.5 eV, ascribed to Al metal and Al^{3+}, respectively. The latter is attributed purely to the oxide film in the pristine Al-NSH, but is also in part due AlCl$_3$ deposited on the sample during immersion pretreatment. The Cl peaks of Al-NSH-18 h are purely anionic, and the two Cl2p$_{3/2}$ peaks are at 197.5 eV and 198.5 eV. The second of these is evidently AlCl$_3$[55] while the lower peak is due to [EMIm]Cl, as reported in Calisi et al.[56] and our own previous results.[57] The Al^{3+} peak of the Al-NSH-18 h is of similar intensity to that of pristine Al, and is lower intensity proportionally due to the addition of Cl2p, N1s, and F1s peaks. Admittedly, it is proportionally larger as compared to the Al-metal peak, as the Al-metal signal is reduced due to the thicker overlayer brought on by deposition products from the salt. The N1s spectrum has a major peak at 401.8 eV and a very minor one at 399.8 eV. The larger one is due to the imidazolium cations of the electrolyte[54] and the minor peak is due to indeterminate neutral C–N species. Both AlCl$_3$ and [EMIm]Cl were observed on the electrode. The only evidence that one of these has decomposed on the electrode is the small N1s peak corresponding to neutral C–N. However, it may also arise from trace remnants of acetonitrile, which was used to wash the electrodes. The F1s spectrum has a major peak at 685.1 eV and a minor one at 688 eV. The latter indicates C–F bonding, though the peak is far too small to be visible in the C1s structure, and the former is trace Al oxyfluorides.[58] A summary and approximate breakdown of the relative signal between spectra can be found in Table 1.

Changes in surface morphology and roughness of cycled Al-NSH foils are shown in Figure 8. The AFM images of the cycled Al foils reveal changes in microstructure when compared to pristine for all performed experiments. The AFM images (Figure 8a) were recorded before and after immersion pretreatment of 6 and 18 h for 100 cycles in [EMIm]Cl/AlCl$_3$ ILE. All cycled Al-NSH foils show mixed features of cracks, fracture, and granular structure evolution after 100 cycles. The mean S$_a$ of the cycled Al-NSH foils with and without immersion pretreatment are shown in Figure 8b as a bar diagram All cycled samples show a significant increase in mean S$_a$ values compared to the Al foil prior to cycling. The Al-NSH-18 h shows the highest increase in mean S$_a$ (889 ± 39 nm). Interestingly, immersion for 6 h (Al-NSH-6 h) revealed less increase (264 ± 31 nm) in surface roughness even compared to the sample without immersion pretreatment (426 ± 35 nm). Although the mean S$_a$ values after immersion prior to cycling are similar, after 100 cycles, it appears that there

ChemSusChem

Research Article
doi.org/10.1002/cssc.202301142

Chemistry
Europe

European Chemical
Societies Publishing

Table 1. A table of binding energies in eV, assignments, and % signal content for each species on each foil surface.

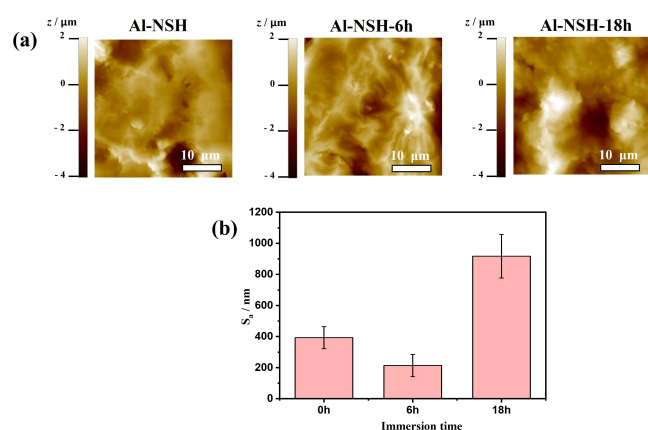| Peak	Pristine Al-NSH		Al-NSH-18 h		Assignment
	Binding energy (eV)	% signal	Binding energy (eV)	% signal	
F1s	–	–	685.1	1.6	Al Oxyfluorides[58]
			688	0.2	C–F
O1s	530.7	11.2	530.8	11.2	Al_2O_3, C=O
	531.9	25.4	532.1	23.9	$Al(OH)_3$, C–O
N1s	–	–	399.8	0.2	neutral C–N[54]
			401.8	2.6	Imidazolium[54,56]
C1s	285	17.1	285	13	C–C
	285.5	6.8	286.3	10.7	C–O, C–N[54]
	289	2.5	289.1	1.5	O–C=O
Cl2$p_{3/2}$	–	–	197.5	1	[EMIm]Cl[56]
			198.5	2.1	$AlCl_3$ [55]
Al2$p_{3/2}$	71.1	12.8	71	7.6	Al metal
	74.2	24.2	74.3	24.4	Al^{3+}

Figure 8. (a) AFM topography images of cycled non-pretreated Al-NSH, Al-NSH-6 h, Al-NSH-18 h, (b) Bar graph of mean S_a values comparison with respect to surface roughness. Error bars reflect standard deviations from data for three different spots at one sample.

Figure 9. CV recorded on the pristine Al-NSH after 500 cycles in [EMIm]Cl/ $AlCl_3$ ILE. Al wire is used as a quasi-reference electrode.

Figure 10. SEM images of the cycled Al-NSH after 500 cycles in [EMIm]Cl/ $AlCl_3$ ILE.

is an effect of the longer pretreatment time, generating more active sites for Al redox reaction (Figure 3b).

Figure 9 displays the long-term cycling behavior of Al-NSH in order to get more insights into electrode aging. After 300 cycles, due to the high polarization, i.e., a drastic increase in resistance, the Al plating and stripping peaks shift to the lower and higher potentials, respectively. Both observed anodic and cathodic polarization can be attributed to the Al pulverization, particularly severe corrosion. With cycling, the generation of active sites and the continuous Al metal and oxide removal result in accelerated local corrosion and subsequent electrode pulverization. As presented in Figure 10, the dendritic Al deposition on the Al surface is a crucial factor affecting Al plating process and corrosion during long cycling. Al electrode pulverization is the consequence of dendritic Al deposition, owning to a possible heterogeneous current distribution. Current flow is mainly happening within the generated active sites (with deep pitting corrosion), making an unequal current
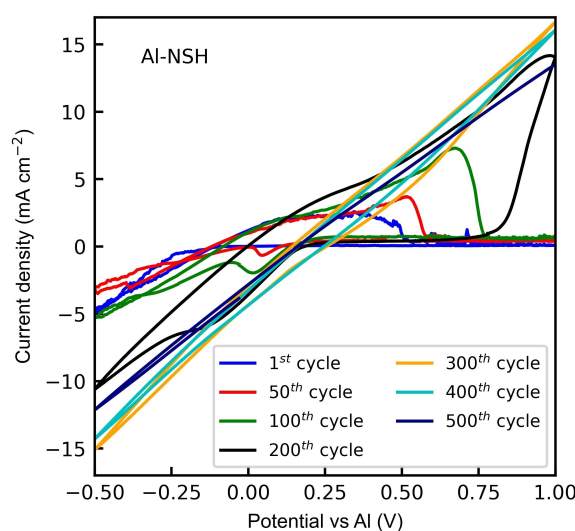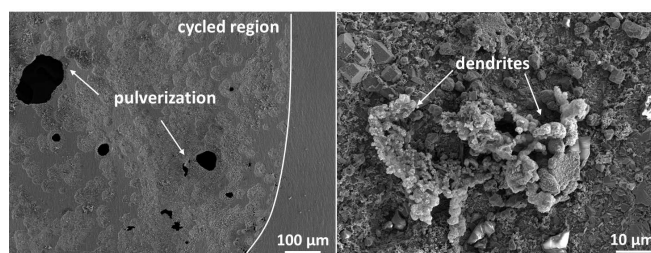
distribution. The SEM images (Figure 10) of the cycled Al-NSH reveal the severe corrosion and pulverization due to the large amount of metallic Al utilization during the stripping process. The Al dendrites point to the consumption of active Al and,

ChemSusChem

Research Article
doi.org/10.1002/cssc.202301142

Chemistry
Europe
European Chemical
Societies Publishing

consequently, an unstable electrode/electrolyte interface. Moreover, dendritic Al deposition with a pebble-like shape is a result of the unremoved Al_2O_3 film covering the Al surface. Both, pebble and sphere-like morphologies of Al dendrites are observed. The latter shape of the Al dendrites is the outcome of the increased current density during long cycling (can be seen in recorded CV (Figure 9). EDX results proved the occurred galvanic corrosion as Fe, an impurity in Al foil, was observed on the severe corrosion sites of the Al surface (Figure S4). Figure 11 shows the AFM image of the Al foil after 500 cycles without prior immersion pretreatment. The observed granular morphology is in line with the SEM image (Figure 10 showing dendritic Al deposition as well as corrosion and pulverization due to the long cycling processes. The roughness parameters are given in a bar diagram in Figure 11a. The decreased S_a (299 ± 20 nm) after 500 cycles is in agreement with the SEM images and recorded CV. We would have expected that longer cycling (comparing S_a values for non-pretreated samples of 500 cycled Al foil and 100 cycled Al foil (426 ± 35 nm)) would further increase the S_a values, which was not observed in our studies. This may be related to the limited number of examined samples.

In addition, nanomechanical properties of the Al foils without any pretreatment were evaluated in dependence of cycling. Figure 12 (a) shows the bar graph of nanomechanical properties of the pristine and Al-NHS sample after 100 cycles both without pretreatment in $[EMIm]Cl/AlCl_3$ ILE; the recorded corresponding AFM images (topography, adhesion force, deformation and Young's modulus) are shown in Figure 12b. It should be noted that these images and the obtained data reflect trends rather than absolute values for the nanomechanical properties, given the complex nature and morphology of the pristine Al-NSH and cycled samples. Notable is the decrease in adhesion force after cycling. For the pristine Al-NSH, an adhesion force 193.89 ± 24.24 nN ($n = 3$) was obtained, which is significantly decreased (by ca. 87%) after 100 cycles to 24.24 ± 1.57 nN ($n = 3$), respectively. The used diamond-coated AFM probes are oxygen-terminated and hydrophilic in nature.[59] Related to the XPS data (Figure 7), the hydrophilic O-terminated diamond probe shows stronger adhesion with the surface groups (Al_2O_3, $Al(OH)_3$) of the pristine sample, whereas cycling leads to changes e.g., partial removal of the passivation layer and formation of corrosion products. In addition, the surface roughness increases with cycling, which may have additional effects,[60] resulting in the observed decrease in adhesion. Also,
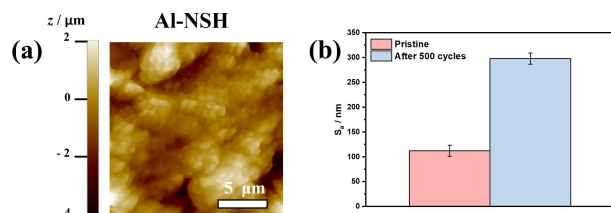

Figure 11. (a) AFM topographic images of the cycled Al-NSH after 500 cycles. (b) Bar graph of mean S_a values. Error bars reflect standard deviations from data for three different spots at one sample.
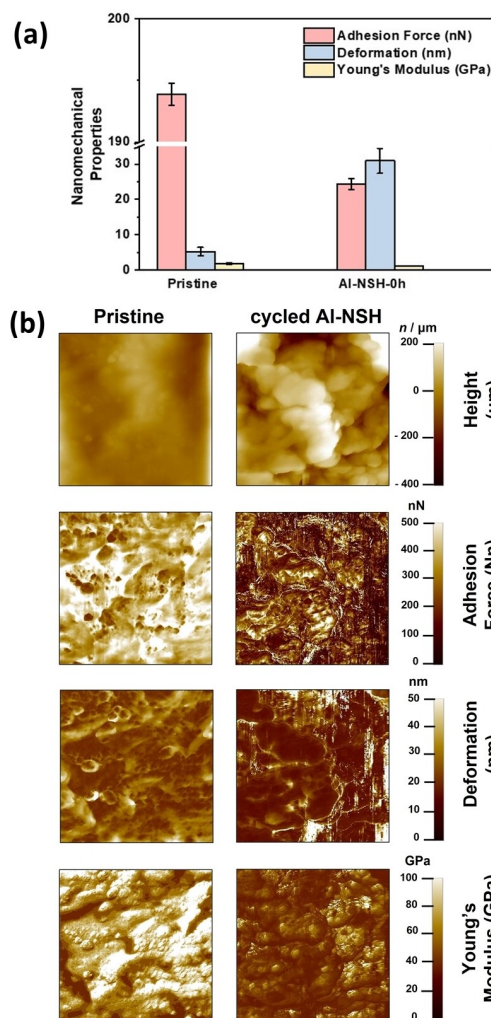

Figure 12. (a) Summary of the nanomechanical characterization results before and after cycling (without any pretreatment). Nanomechanical properties of pristine and cycled Al foil in $[EMIm]Cl/AlCl_3$ ILE. Error bars reflect standard deviations from data for three different spots at one sample. (b) Nanomechanical characterization of pristine and cycled Al-NSH (non-pretreated), recorded image of height, adhesion force, deformation, and Young's modulus. Scale = 5 X 5 µm^2.

the deformation values change after cycling. The observed values of deformation for the cycled Al-NSH show an increase of 30.94 ± 3.52 nm ($n = 3$) when compared to pristine 5.19 ± 1.18 nm ($n = 3$). We associate these changes to the corrosion reaction during the stripping process, leading to changes in the surface microstructure (as discussed in SEM, Figure 5). Also, the Young's modulus of the Al foil of pristine was determined as 1.88 ± 0.23 GPa ($n = 3$), which was reduced to 1.13 ± 0.1 GPa ($n = 3$) after 100 cycles. The decrease in Young's modulus value after 100 cycles may be associated with the formation of inorganic salts. The decrease in both adhesion force and Young's modulus of the cycled Al foil after 100 cycles may be related to the changes in the microstructure of the surface by partial/complete removal of the passivation layer, Al_2O_3 from the surface and subsequent deposition of Al dendrites on the surface of the Al foil during plating /stripping process in $[EMIm]Cl/AlCl_3$ ILE. The nanomechanical properties of such

complex samples are influenced by many factors, such as changes in surface morphology by the removal of the passivation layer, formation of an interphase layer and corrosion processes along with the deposition of products.

Conclusions

This study demonstrated how the Al_2O_3 film, particularly the surface properties (roughness and microstructure) of Al foils, affect the electrochemical behavior and electrode aging on two sides of Al foil as a potential negative electrode in RABs. The initial surface properties of the Al electrode, the immersion duration (pretreatment), and the utilized mass of [EMIm]Cl/AlCl₃ should be taken into account while exploring the role of the surface modification on Al plating/stripping. The acidity of the electrolyte as well as its utilized mass for immersion pretreatment alter the Al surface properties. In addition, the impact of the immersion pretreatment on Al cycling performance has been explored here. Benefiting from the optimum immersion pretreatment time (18 h), the pretreated aluminum metal foil can be reversibly cycled from the 1st cycle. Our findings indicated that the pristine and pretreated Al foil surfaces' non-shiny side compared to the shiny side are more susceptible to be attacked by the aluminum chloride complex and to undergo surface changes. As a result, the surface properties govern the electron and ion transport at the Al anode–electrolyte contact as well as the electrode aging/degradation. The mechanical surface properties of cycled Al have been studied. However, since the studied samples are very complex, we presented a qualitative trend and further work, including in-situ studies and modeling, should be done in the future.

Experimental Section

Materials

In this study, [EMIm]Cl/AlCl₃ with the molar ratio of 1:1.5 as a conventional IL electrolyte in Al-ion batteries was prepared by slowly adding the appropriate amount of AlCl₃ (Anhydrous, Sigma Aldrich, 99.99%) to [EMIm]Cl (Sigma Aldrich, ≥95%) while stirring at room temperature (28 to 30°C) with magnet bar inside the argon-filled glovebox (MBraun, <0.5 ppm O_2, <0.5 ppm H_2O). When AlCl₃, a Lewis acid, interacts with Cl⁻ as a Lewis base, it transforms a solid mixture into a liquid state, forming $AlCl_4^-$ ions, balanced by EMIM⁺ cations.[44] The Aluminum foil (0.025 mm thickness, 99.0% purity, and annealed temper) was purchased from Goodfellow. Anhydrous acetonitrile (99.8%) was purchased from Sigma Aldrich.

Electrochemical setup

All the electrochemical measurements were carried out in an argon-filled glovebox (MBraun, <0.5 ppm O_2, <0.5 ppm H_2O). Cyclic voltammetry (CV) was recorded in a sealed and airtight TSC surface cell purchased from rhd Instruments Company. This cell is equipped with a glassy carbon (GC) disc as a counter electrode, and an Al wire quasi-reference electrode. Al foil was taken as a working electrode in this cell configuration. Before each experiment, the GC electrode was polished with 250 nm diamond polishing paste, then washed with deionized water, and finally dried. The Al quasi-reference electrode was rinsed in a mixture of $H_2SO_4/H_3PO_4/HNO_3$ (25/70/5 by volume) for 5 to 15 min to remove any residual oxide, dirt, or contamination.[61] Furthermore, the reference electrode was washed with acetone, dried, and stored under a vacuum before each measurement. All cell parts were dried in an oven at 60–80°C, then transferred to the argon-filled glovebox before each cell assembly. CV curves (100 and 500 cycles) were recorded with a biologic potentiostat (VMP12) at 25°C, with the scan rate of 20 mV s⁻¹ in a potential range of −0.5–0 V vs. Al in [EMIm]Cl/AlCl₃ (1:1.5) ILE.

Ex-situ characterization of Al electrodes

The preparation and handling for the *ex-situ* characterization of Al foils were done inside an argon-filled glovebox (MBraun, <0.5 ppm O_2, <0.5 ppm H_2O). Pretreated and cycled Al foils were washed three times with anhydrous acetonitrile inside the glovebox, and then they were dried under vacuum for 12 h in a glass oven (BÜCHI Glass Oven B-585). Pretreated electrodes were prepared as follows: Al foils were immersed in 900 μl of [EMIm]Cl/AlCl₃ (1:1.5) for 6 and 18 h. Scanning electron microscope (SEM) images of the pristine, pretreated, and cycled Al foils were collected by using JEOL JSM 7500F instruments with an acceleration voltage of 5 kV. The elemental analysis of the Al foil was done by energy-dispersive X-ray spectroscopy (EDX) with an acceleration voltage of 10 kV. All atomic force microscopy (AFM) measurements of the pristine, pretreated, and cycled Al foil were performed with an AFM microscope (Park NX10, Park Systems) located inside an argon-filled glovebox (Unilab, MBraun, O_2, H_2O <0.1 ppm). Morphological changes and roughness of pristine, pretreated, and cycled Al foil were characterized using a closed-loop scanner in non-contact mode and were measured before and after 100 and 500 cycles. Non-contact mode experiments were performed with high aspect ratio silicon AFM probes (PPP-NCHR, NanoWorld AG, Switzerland) with a resonant frequency of 330 kHz and a nominal tip radius of 10 nm. Images were recorded at a scan speed of 0.7 Hz. The force constant of the cantilevers ($k=42$ N m⁻¹) was determined using the thermal noise method.[62] The nanomechanical properties of the pristine and cycled electrodes were determined with diamond-coated AFM probes (DT-NCHR, Nanoworld AG, Switzerland) with a resonant frequency of 400 kHz and a tip radius of 10 nm. Images were recorded at a scan speed of 0.2 Hz. Roughness data (mean surface, arithmetic roughness (S_a)) and nanomechanical data were analyzed using Park's imaging processing tool for Scanning Probe Microscopy (SPM) data (XEI 5.2, Park Systems). The pinpoint nanomechanical mode eliminates lateral shear forces, which drastically reduces potential damage of the surface. Pinpoint mode was used to simultaneously image surface topography along with Young's modulus, deformation, and adhesion. The used cantilevers were first calibrated using a piece of Si wafer before the Al samples were measured. X-ray photoelectron spectroscopy (XPS) measurements of the pristine and pretreated Al foil were done with a Specs EnviroESCA NAP-XPS[63] (without making use of the NAP features, so at roughly 10^{-5} mbar) via a nitrogen-filled glovebox (GS, <5 ppm O_2, <0.5 ppm H_2O). All Al electrodes are abbreviated as Al-NSH (non-shiny side of Al foil), Al-SH (shiny side of Al foil), Al-NSH-6 h (non-shiny pretreated for 6 h), and Al-NSH-18 h (non-shiny pretreated for 18 h).

Supporting Information

Acknowledgements

Conflict of Interests

The authors declare no conflict of interest.

Data Availability Statement

The data that support the findings of this study are openly available in Repository KIT open at https://doi.org/10.35097/1659.

[1] B. Dunn, H. Kamath, J.-M. Tarascon, *Science (1979)* **2011**, DOI 10.1126/science.1212741.
[2] W.-J. Zhang, *J. Power Sources* **2011**, *196*, 13–24.
[3] Y. Hu, D. Sun, B. Luo, L. Wang, *Energy Technol.* **2019**, *7*, 86–106.
[4] A. Eftekhari, P. Corrochano, *Sustain. Energy Fuels* **2017**, *1*, 1246–1264.
[5] M. Jiang, C. Fu, P. Meng, J. Ren, J. Wang, J. Bu, A. Dong, J. Zhang, W. Xiao, B. Sun, *Adv. Mater.* **2022**, *34*, 2102026.
[6] Q. Li, N. J. Bjerrum, *J. Power Sources* **2002**, *110*, 1–10.
[7] G. A. Elia, K. Marquardt, K. Hoeppner, S. Fantini, R. Lin, E. Knipping, W. Peters, J.-F. Drillet, S. Passerini, R. Hahn, *Adv. Mater.* **2016**, *28*, 7564–7579.
[8] S. Zaromb, *J. Electrochem. Soc.* **1962**, *109*, 1125.
[9] Y.-J. Cho, I.-J. Park, H.-J. Lee, J.-G. Kim, *J. Power Sources* **2015**, *277*, 370–378.
[10] L. Qingfeng, H. A. Hjuler, R. W. Berg, N. J. Bjerrum, *J. Electrochem. Soc.* **1990**, *137*, 593–598.
[11] E. Berretti, A. Giaccherini, S. Martinuzzi, M. Innocenti, T. Schubert, F. Stiemke, S. Caporali, *Materials* **2016**, *9*, 719.
[12] H. Yang, F. Wu, Y. Bai, C. Wu, *J. Energy Chem.* **2020**, *45*, 98–102.
[13] H. Chen, H. Xu, B. Zheng, S. Wang, T. Huang, F. Guo, W. Gao, C. Gao, *ACS Appl. Mater. Interfaces* **2017**, *9*, 22628–22634.
[14] M.-C. Lin, M. Gong, B. Lu, Y. Wu, D.-Y. Wang, M. Guan, M. Angell, C. Chen, J. Yang, B.-J. Hwang, H. Dai, *Nature* **2015**, *520*, 324–328.
[15] M. Jäckle, K. Helmbrecht, M. Smits, D. Stottmeister, A. Groß, *Energy Environ. Sci.* **2018**, *11*, 3400–3407.
[16] Y. Long, H. Li, M. Ye, Z. Chen, Z. Wang, Y. Tao, Z. Weng, S.-Z. Qiao, Q.-H. Yang, *Energy Storage Mater.* **2021**, *34*, 194–202.
[17] S. Choi, H. Go, G. Lee, Y. Tak, *Phys. Chem. Chem. Phys.* **2017**, *19*, 8653–8656.
[18] E.-S. Lee, S.-H. Huh, S.-H. Lee, S.-H. Yu, *ACS Sustainable Chem. Eng.* **2023**, *11*, 2014–2032.
[19] D.-M. She, W.-L. Song, J. He, N. Li, H. Chen, S. Jiao, D. Fang, *J. Electrochem. Soc.* **2020**, *167*, 130530.
[20] H. Chen, H. Xu, B. Zheng, S. Wang, T. Huang, F. Guo, W. Gao, C. Gao, *ACS Appl. Mater. Interfaces* **2017**, *9*, 22628–22634.
[21] S. Choi, H. Go, G. Lee, Y. Tak, *Phys. Chem. Chem. Phys.* **2017**, *19*, 8653–8656.
[22] H. Go, M. R. Raj, Y. Tak, G. Lee, *Electroanalysis* **2022**, *34*, 1308–1317.
[23] H. Wang, S. Gu, Y. Bai, S. Chen, N. Zhu, C. Wu, F. Wu, *J. Mater. Chem. A* **2015**, *3*, 22677–22686.
[24] F. Wu, N. Zhu, Y. Bai, Y. Gao, C. Wu, *Green Energy & Environ.* **2018**, *3*, 71–77.
[25] H. Wang, S. Gu, Y. Bai, S. Chen, F. Wu, C. Wu, *ACS Appl. Mater. Interfaces* **2016**, *8*, 27444–27448.
[26] S. Choi, H. Go, G. Lee, Y. Tak, *Phys. Chem. Chem. Phys.* **2017**, *19*, 8653–8656.
[27] H. Wang, S. Gu, Y. Bai, S. Chen, N. Zhu, C. Wu, F. Wu, *J. Mater. Chem. A* **2015**, *3*, 22677–22686.
[28] X. Zhan, J. F. Bonnett, M. H. Engelhard, D. M. Reed, V. L. Sprenkle, G. Li, *Adv. Energy Mater.* **2020**, *10*, DOI 10.1002/aenm.202001378.
[29] F. Wu, N. Zhu, Y. Bai, Y. Gao, C. Wu, *Green Energy & Environ.* **2018**, *3*, 71–77.
[30] X. Wang, L. Chen, L. Wang, Q. Fan, D. Pan, J. Li, F. Chi, Y. Xie, S. Yu, C. Xiao, F. Luo, J. Wang, X. Wang, C. Chen, W. Wu, W. Shi, S. Wang, X. Wang, *Sci. China Chem.* **2019**, *62*, 933–967.
[31] Z. J. Karpinski, R. A. Osteryoung, *Inorg. Chem.* **1984**, *23*, 1491–1494.
[32] N. Takami, N. Koura, *Electrochim. Acta* **1988**, *33*, 1137–1142.
[33] D. Ma, D. Yuan, C. Ponce de León, Z. Jiang, X. Xia, J. H. Pan, *Energy Environ.* **2021**, DOI 10.1002/eem2.12301.
[34] M.-C. Lin, M. Gong, B. Lu, Y. Wu, D.-Y. Wang, M. Guan, M. Angell, C. Chen, J. Yang, B.-J. Hwang, H. Dai, *Nature* **2015**, *520*, 324–328.
[35] D. Muñoz-Torrero, J. Palma, R. Marcilla, E. Ventosa, *Dalton Trans.* **2019**, *48*, 9906–9911.
[36] S. Choi, H. Go, G. Lee, Y. Tak, *Phys. Chem. Chem. Phys.* **2017**, *19*, 8653–8656.
[37] S. Zein El Abedin, P. Giridhar, P. Schwab, F. Endres, *Electrochem. Commun.* **2010**, *12*, 1084–1086.
[38] L. C. Loaiza, N. Lindahl, P. Johansson, *J. Electrochem. Soc.* **2023**, DOI 10.1149/1945-7111/acb108.
[39] D. Lee, G. Lee, Y. Tak, *Nanotechnology* **2018**, *29*, 36LT01.
[40] M. Textor, M. Amstutz, *Anal. Chim. Acta* **1994**, *297*, 15–26.
[41] N. Sabi, K. Palanisamy, F. Rahide, S. Daboss, C. Kranz, S. Dsoke, *Batteries & Supercaps* **2023**, DOI 10.1002/batt.202300298.
[42] L. Gjønnes, *Wear* **1996**, *192*, 216–227.
[43] H. Sun, W. Wang, Z. Yu, Y. Yuan, S. Wang, S. Jiao, *Chem. Commun.* **2015**, *51*, 11892–11895.
[44] K. V. Kravchyk, C. Seno, M. V. Kovalenko, *ACS Energy Lett.* **2020**, *5*, 545–549.
[45] T. Tsuda, G. R. Stafford, C. L. Hussey, *J. Electrochem. Soc.* **2017**, *164*, H5007–H5017.
[46] P. K. Lai, M. Skyllas-Kazacos, *Electrochim. Acta* **1987**, *32*, 1443–1449.
[47] Y. Chao-Cheng, *Mater. Chem. Phys.* **1994**, *37*, 355–361.
[48] Y. Zhao, T. J. VanderNoot, *Electrochim. Acta* **1997**, *42*, 3–13.
[49] S. Zein El Abedin, E. M. Moustafa, R. Hempelmann, H. Natter, F. Endres, *ChemPhysChem* **2006**, *7*, 1535–1543.
[50] S. Xia, X.-M. Zhang, K. Huang, Y.-L. Chen, Y.-T. Wu, *J. Electroanal. Chem.* **2015**, *757*, 167–175.
[51] O. M. E. Ylivaara, X. Liu, L. Kilpi, J. Lyytinen, D. Schneider, M. Laitinen, J. Julin, S. Ali, S. Sintonen, M. Berdova, E. Haimi, T. Sajavaara, H. Ronkainen, H. Lipsanen, J. Koskinen, S.-P. Hannula, R. L. Puurunen, *Thin Solid Films* **2014**, *552*, 124–135.
[52] N. Fairley, V. Fernandez, M. Richard-Plouet, C. Guillot-Deudon, J. Walton, E. Smith, D. Flahaut, M. Greiner, M. Biesinger, S. Tougaard, D. Morgan, J. Baltrusaitis, *Appl. Sur. Sci. Adv.* **2021**, *5*, 100112.
[53] L. C. Loaiza, N. Lindahl, P. Johansson, *J. Electrochem. Soc.* **2023**, *170*, 030512.
[54] S. Caporali, U. Bardi, A. Lavacchi, *J. Electron Spectrosc. Relat. Phenom.* **2006**, *151*, 4–8.
[55] H. Xu, T. Bai, H. Chen, F. Guo, J. Xi, T. Huang, S. Cai, X. Chu, J. Ling, W. Gao, Z. Xu, C. Gao, *Energy Storage Mater.* **2019**, *17*, 38–45.
[56] N. Calisi, S. Martinuzzi, A. Giaccherini, C. S. Pomelli, L. Guazzelli, S. Caporali, *J. Electron Spectrosc. Relat. Phenom.* **2021**, *247*, 147034.
[57] F. Rahide, J. K. Flowers, J. Hao, H. S. Stein, H. Ehrenberg, S. Dsoke, *submitted to Journal of The Electrochemical Society and under revision* **2023**.
[58] D. S. Kim, Y. Y. Yu, K. Char, *J. Appl. Phys.* **2004**, *96*, 2278–2285.

[59] R. Hoffmann, A. Kriele, H. Obloh, J. Hees, M. Wolfer, W. Smirnov, N. Yang, C. E. Nebel, *Appl. Phys. Lett.* **2010**, *97*, DOI 10.1063/1.3476346.

[60] L. A. Thimons, A. Gujrati, A. Sanner, L. Pastewka, T. D. B. Jacobs, *Exp. Mech.* **2021**, *61*, 1109–1120.

[61] T. Mandai, P. Johansson, *J. Mater. Chem. A* **2015**, DOI 10.1039/c5ta01760b.

[62] J. L. Hutter, J. Bechhoefer, *Rev. Sci. Instrum.* **1993**, *64*, 1868–1873.

[63] P. M. Dietrich, S. Bahr, T. Yamamoto, M. Meyer, A. Thissen, *J. Electron Spectrosc. Relat. Phenom.* **2019**, *231*, 118–126.

[64] F. Rahide, K. Palanisamy, J. K. Flowers, J. Hao, H. S. Stein, C. Kranz, H. Ehrenberg, S. Dsoke, *submitted to ChemSusChem and under revision* **2023**.